Front. Optoelectron. China 2008, 1(1–2): 3–13
DOI 10.1007/s12200-008-0030-4

RESEARCH ARTICLE

Experimental realization of 40 Gbit/s single-to-single and single-to-dual channel wavelength conversions in $LiNbO_3$ waveguides with two-pump configuration

Jian WANG, Junqiang SUN (✉), Qizhen SUN, Weiwei ZHANG, Zhefeng HU, Xinliang ZHANG, Dexiu HUANG

Wuhan National Laboratory for Optoelectronics, School of Optoelectronic Science and Engineering, Huazhong University of Science and Technology, Wuhan 430074, China

Abstract An all-optical 40 Gbit/s tunable single-to-single channel wavelength conversion is experimentally realized based on cascaded sum- and difference-frequency generation (cSFG/DFG) in periodically poled $LiNbO_3$ (PPLN) waveguides. By employing two tunable filters to effectively suppress the amplified spontaneous emission (ASE) noise, both wavelength down- and up-conversions are simultaneously observed. We also propose and verify a novel cSFG/DFG-based single-to-dual channel wavelength conversion by setting two pumps (pump1, pump2) close to each other or pump2 and the signal close to each other. For the latter, two kinds of cSFG/DFG schemes are both demonstrated. The dependence of the conversion efficiencies of two channel idler waves on pump1 wavelength is discussed. The wavelength relationships between two channel idler waves and the three incident waves are investigated in detail theoretically as well as experimentally.

Keywords nonlinear optics, optical communications, periodically poled $LiNbO_3$ (PPLN), cascaded sum- and difference-frequency generation (cSFG/DFG), single-to-dual channel wavelength conversion

1 Introduction

Periodically poled $LiNbO_3$ (PPLN) waveguides are considered to be the most promising components for all-optical wavelength conversion, which is the essential function of future dense wavelength-division-multiplexed (DWDM) optical networks [1]. Wavelength converters based on second-order nonlinearities in PPLN waveguides have attracted considerable interest in recent years [2–29]. They fulfill the requirements of an ideal wavelength converter, such as ultra-fast response for high-speed wavelength conversion, complete transparency and independence of bit rate and data format, negligible spontaneous emission noise, large conversion bandwidth, high conversion efficiency, no intrinsic frequency chirp and low crosstalk, etc. Three approaches, called direct difference-frequency generation (DFG) [2–4], cascaded second-harmonic generation and difference-frequency generation (cSHG/DFG) [4–13], and cascaded sum- and difference-frequency generation (cSFG/DFG) [14–29] have been proposed to perform the wavelength conversion within the 1.5-μm band, respectively. In the direct DFG-based wavelength conversion [2–4], it is difficult to simultaneously launch the pump in the 0.77-μm band and the signal in the 1.5-μm band into the waveguide. This can be solved by using cSHG/DFG [4–13] or cSFG/DFG [14–29], during which all the incident waves are within the 1.5-μm band. In the cSHG/DFG processes [4–10], one pump wave in the 1.5-μm band is used to yield a frequency-doubled wave in the 0.77-μm band which simultaneously interacts with the 1.5-μm band signal wave to generate an idler wave in the 1.5-μm band. For a fixed input signal wavelength, the wavelength of the output idler wave is decided by the input pump wavelength. However, due to the very small pump-wavelength tolerance (~0.3 nm) restricted by the quasi-phase matching (QPM) condition [4], it is practically impossible to realize the tunable wavelength conversion based on cSHG/DFG. In order to achieve optically tunable wavelength conversion, which is required to enhance the flexibility of future network systems, cSFG/DFG employing two pumps is proposed and demonstrated by Min Y. H. [16], Yamawaku J. [17], Lee Y. L. [18,19], and Yu S. [20], respectively. In their schemes, one pump (pump1) and the signal, both within the 1.5-μm band, generate the sum-frequency wave in the 0.77-μm

Received August 5, 2007; accepted October 15, 2007

E-mail: jqsun@mail.hust.edu.cn

band. Meanwhile, the second pump (pump2) in the 1.5-μm band interacts with the sum-frequency wave to generate an idler wave in the 1.5-μm band by DFG. It is noted that SFG takes place between one pump and the signal, and the tunable operation can be simply implemented by changing the second pump wavelength. Actually, there is another cSFG/DFG-based conversion scheme with SFG occurring between two pumps [21–24] proposed by Xu C. Q. [21] and Chen B. [22]. We have experimentally demonstrated the latter cSFG/DFG-based wavelength conversion between picosecond pulses [24]. Noting that most previous cSFG/DFG schemes employed continuous wave (CW) signals [18–23] or operated at relatively low speed [16,17], it did not take full advantage of the ultra-fast nonlinear response characteristic of the PPLN waveguide. Moreover, the amplified spontaneous emission (ASE) noise was strong making the wavelength down- and up-conversions difficult to be simultaneously observed in the experiments [16–19,21,24]. In addition, although the two kinds of cSFG/DFG schemes above have been demonstrated respectively, their combination, i.e., simultaneous observation of two nonlinear cSFG/DFG interactions, however, has not been reported before.

In this paper, we propose and demonstrate the high-speed single-to-single and single-to-dual channel wavelength conversions based on cSFG/DFG. 40 Gbit/s non-return-to-zero (NRZ) signal is adopted. One high-power erbium-doped fiber amplifier (HP-EDFA) with two tunable filters are employed to amplify two pumps and effectively suppress the ASE noise. As a result, on one hand, 40 Gbit/s tunable single-to-single channel wavelength down- and up-conversions are both experimentally observed. On the other hand, when the wavelengths of two pumps are close to each other or the signals of one pump and the signal are close to each other, it is also possible to realize the single-to-dual channel wavelength conversion. Particularly, two kinds of cSFG/DFG interactions are simultaneously observed in the experiment.

The paper is organized as follows: Sect. 2 explains the concept and the working principle of single-to-single and single-to-dual channel wavelength conversions based on cSFG/DFG. Section 3 presents the experimental setup. Experimental results and discussions are included in Sect. 4. Finally, the paper is concluded in Sect. 5.

2 Concept and working principle

Figure 1 illustrates the working principle of tunable single-to-single channel wavelength conversion based on cSFG/DFG. Two pumps are employed. One pump (λ_{P1}) interacts with the input signal (λ_S) through the nonlinear SFG effect under the QPM condition and the sum-frequency wave (λ_{SF}) is generated. Meanwhile, the second pump (λ_{P2}) is mixed with the sum-frequency wave to generate an idler wave (λ_i) by the subsequent DFG process. As a result, the information carried by the signal wavelength is completely copied onto the wavelength of the converted idler wave. According to the law of energy conservation, wavelengths of the interacting waves are governed by the following expressions:

$$\text{SFG: } 1/\lambda_{SF} = 1/\lambda_S + 1/\lambda_{P1}, \tag{1}$$

$$\text{DFG: } 1/\lambda_i = 1/\lambda_{SF} - 1/\lambda_{P2}, \tag{2}$$

$$\text{cSFG/DFG: } 1/\lambda_i = 1/\lambda_S + 1/\lambda_{P1} - 1/\lambda_{P2}. \tag{3}$$

From Eqs. (1)–(3), for a fixed input signal wavelength, the wavelength of pump1 is first tuned to satisfy the QPM condition for the SFG process. Then, as shown in Figs. 1(a)–1(d), the variable output idler wavelength can be obtained by changing the wavelength of pump2, which corresponds to the tunable wavelength conversion.

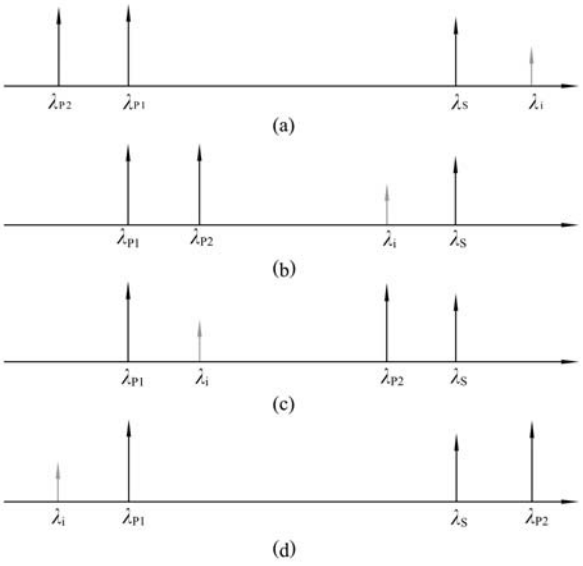

Fig. 1 Working principle of tunable single-to-single channel wavelength conversion based on cSFG/DFG

Figure 2 shows the concept and operating principle of the cSFG/DFG-based single-to-dual channel wavelength conversion. Compared with single-to-single channel wavelength conversion mentioned above, the wavelength of pump2 is set close to the pump1 wavelength or near the signal wavelength. As shown in Figs. 2(a) and 2(b), when pump2 wavelength moves towards the pump1 wavelength, the SFG process takes place not only between pump1 and the signal, but also between pump2 and the signal. Consequently, two sum-frequency waves are generated and two output idler waves are obtained. Thus, single-to-dual channel wavelength conversion is realized. Similarly, when the wavelength of pump2 gets close to the signal

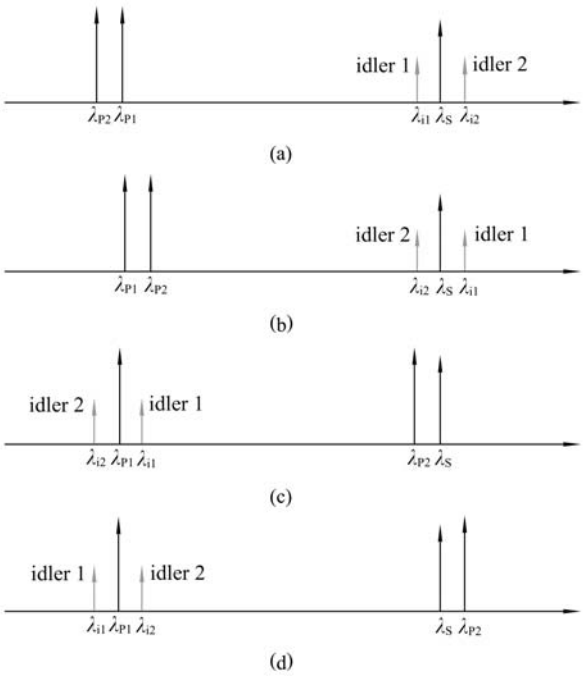

Fig. 2 Concept and working principle of single-to-dual channel wavelength conversion based on cSFG/DFG

wavelength, as shown in Figs. 2(c) and 2(d), the SFG process simultaneously occurs between pump1 and the signal as well as between pump1 and pump2. As a result of which, two output idler waves are achieved and the single-to-dual channel wavelength conversion can also be implemented. Note that two channel idler wavelengths in Figs. 2(a) and 2(b) satisfy the following relationships:

$$\text{Channel 1:} \quad 1/\lambda_{i1} = 1/\lambda_S + 1/\lambda_{P2} - 1/\lambda_{P1}, \tag{4}$$

$$\text{Channel 2:} \quad 1/\lambda_{i2} = 1/\lambda_S + 1/\lambda_{P1} - 1/\lambda_{P2}. \tag{5}$$

And the single-to-dual channel wavelength conversion in Figs. 2(c) and 2(d) can be described as follows:

$$\text{Channel 1:} \quad 1/\lambda_{i1} = 1/\lambda_S + 1/\lambda_{P1} - 1/\lambda_{P2}, \tag{6}$$

$$\text{Channel 2:} \quad 1/\lambda_{i2} = 1/\lambda_{P1} + 1/\lambda_{P2} - 1/\lambda_S. \tag{7}$$

Remarkably, from Eqs. (4) and (5), it is found that two channel idler waves are generated by the same kind cSFG/DFG interactions with the SFG process occurring between the signal and one of the two pumps. By comparison, from Eqs. (6) and (7), it is noticed that two kinds of cSFG/DFG schemes, depending on whether the SFG process occurs between one pump and the signal or between two pumps, are both included in Figs. 2(c) and 2(d).

It is worth noting that the only difference between Figs. 1 and 2 is the position of the pump2 wavelength. In fact, when the wavelength of pump2 is far from both pump1 and the signal wavelengths, the SFG interactions between pump2 and the signal in Figs. 1(a) and 1(b), as well as between pump2 and pump1 in Figs. 1(c) and 1(d), can be ignored completely as the QPM condition is severely phase-mismatched. On the contrary, when the pump2 wavelength is close to pump1 or the signal wavelength, since the wavelengths of pump1 and the signal meet the QPM condition for the SFG process, the SFG interactions between pump2 and the signal in Figs. 2(a) and 2(b), as well as between pump2 and pump1 in Figs. 2(c) and 2(d), are slightly phase-mismatched. As a consequence, Fig. 1 presents the tunable single-to-single channel wavelength conversion, while Fig. 2 exhibits the single-to-dual channel wavelength conversion.

3 Experimental setup

The experimental setup is shown in Fig. 3. Two CW pumps (λ_{P1} and λ_{P2}) are generated from two tunable external cavity lasers (ECL1 and ECL2), respectively. The 40 Gbit/s NRZ signal at 1549.7 nm is provided by use of a distributed feedback laser (DFB), a Mach-Zehnder modulator (MZM) and a bit pattern generator (BPG). The wavelengths of the two pumps can be tuned from 1461 to 1555 nm. They are combined together and simultaneously pre-amplified by a HP-EDFA with the small-signal gain of 40 dB and high saturation output power of 30 dBm. And then, in order to effectively suppress the ASE noise originating from the HP-EDFA, two amplified pumps are demultiplexed and individually passed through two tunable filters. By using a 3×1 optical coupler, the signal and the two CW pumps are coupled into the PPLN waveguide and participate in the nonlinear cSFG/DFG interactions. The PPLN waveguide with a length of 50 mm is fabricated by the electric-field poling method and thereafter by the annealing proton-exchanged (APE) process. It has a microdomain period of 14.7 μm, a waveguide width of 12 μm, and an initial proton exchange depth of 0.8 μm. During the experiment, the QPM wavelength for the SHG process is about 1543.2 nm at room temperature. The fiber-to-fiber coupling loss is estimated at about 4.7 dB due to the reflection losses at the uncoated end faces, mode mismatching between the fibers and the PPLN waveguide, and intrinsic waveguide losses. The tuning bandwidth and line width of the tunable filters are 50 and 1 nm, respectively. An inline polarization controller (PC) is inserted into the configuration to enhance the nonlinear interactions in the PPLN waveguide. By appropriately tuning two pump wavelengths, tunable single-to-single channel wavelength conversion and single-to-dual channel wavelength conversion can be realized. The output spectra are monitored by an optical spectrum analyzer (Anritsu MS9710C) with the highest spectral resolution of 0.05 nm, and the temporal waveforms are observed through a communications signal analyzer (Tektronix CSA 8000B).

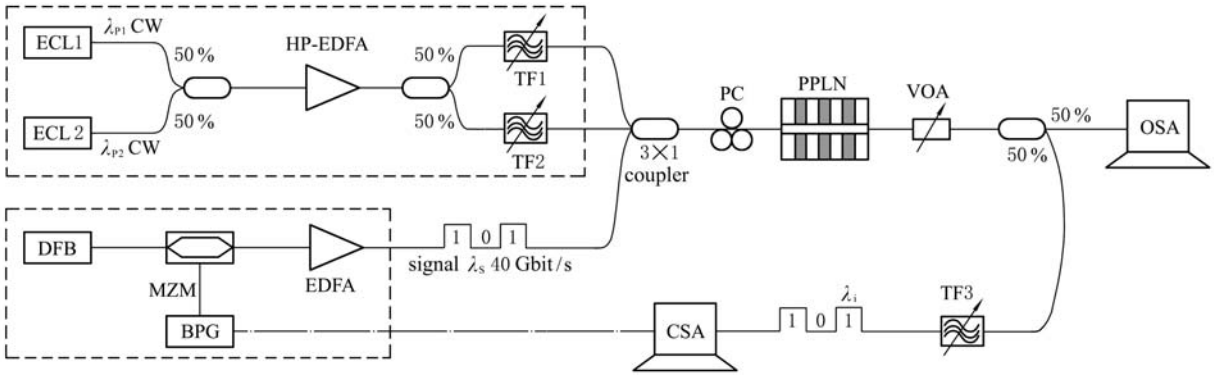

Fig. 3 Experimental setup. (DFB: distributed feedback laser; MZM: Mach-Zehnder modulator; BPG: bit pattern generator; EDFA: erbium-doped fiber amplifier; ECL: external cavity laser; TF: tunable filter; PC: polarization controller; VOA: variable optical attenuator; OSA: optical spectrum analyzer; CSA: communications signal analyzer)

4 Experimental results and discussion

4.1 Tunable single-to-single channel wavelength conversion

We first perform a 40 Gbit/s tunable single-to-single channel wavelength conversion. The optical spectrum at the output of the PPLN waveguide is shown in Fig. 4(a). The wavelength of the input signal is fixed at 1549.7 nm. The first pump (pump1) wavelength is set at 1536.6 nm to meet the QPM condition for the SFG process, generating the sum-frequency wave in the 0.77-μm band, which is shown in Fig. 4(b). Simultaneously, the wavelength of the second pump (pump2) is tuned at 1531.3 nm, interacting with the sum-frequency wave to generate an idler wave at about 1555.4 nm by the DFG

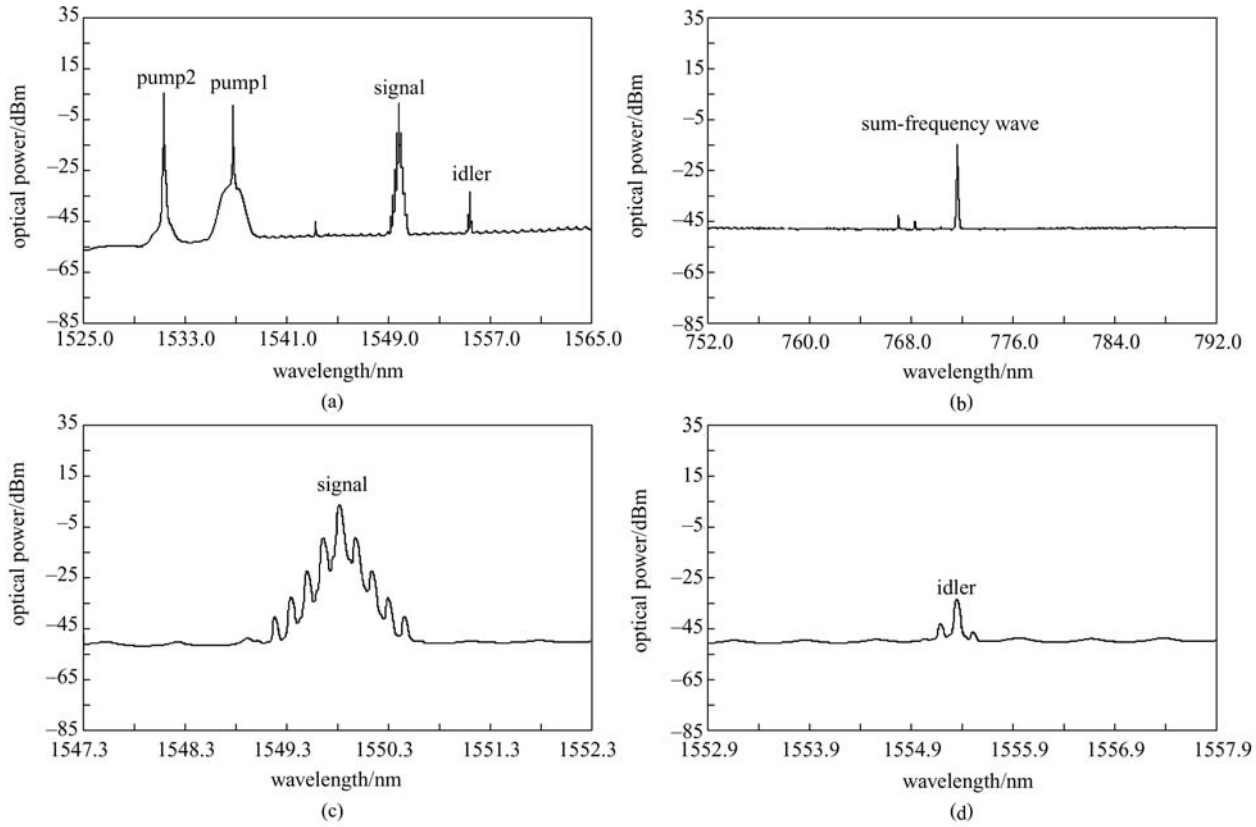

Fig. 4 40 Gbit/s single-to-single channel wavelength conversion. (a) Optical spectrum of the cSFG/DFG-based single-to-single channel wavelength conversion at the output of PPLN waveguide; (b) sum-frequency wave in the 0.77-μm band; (c) detailed optical spectrum of signal; (d) detailed optical spectrum of converted idler

process. Remarkably, the converted idler wave shown in Fig. 4(d) has the similar optical spectrum compared with the input signal shown in Fig. 4(c). This explains the cSFG/DFG-based wavelength conversion from the signal wave to the idler wave. In Fig. 4(a), the powers of pump1 and pump2 at the output of the PPLN waveguide are about 0.71 and 5.56 dBm, respectively. The conversion efficiency is measured at approximately −34.58 dB, which is not very high. However, since the ASE noise over the whole wavelength range from 1525.0 to 1565.0 nm is greatly suppressed, wavelength up-conversion is successfully observed in Fig. 4(a). Figure 5 presents the temporal waveforms of the (R1, R2) output idler and (C1, C2) input signal waves when 40 Gbit/s NRZ signal is employed with different bit stream of (a) "1 0 1 0 1 0 1 0" and (b) "1 0 0 0 1 1 0 0". It can be seen that the information carried by the signal wavelength is completely copied onto the idler wavelength and the wavelength conversion from the signal to the idler is successfully realized.

Figure 6 further illustrates the tunable performance of the cSFG/DFG-based wavelength conversion. The wavelengths of the signal and pump1 are kept at 1549.7 and 1536.6 nm, respectively. The wavelength of pump2 is tuned from 1529.8 to 1554.5 nm (limited by EDFA gain bandwidth and the tunable range of pump2), resulting in the converted idler wavelength from 1556.8 to 1531.9 nm. Approximately, 24.9-nm conversion span is achieved. It is found that the optical spectra shown in Figs. 6(a)–6(d) agree well with the description of the tunable single-to-single channel wavelength conversion shown in Figs. 1(a)–1(d).

Since two tunable filters are utilized in the wavelength converter, the ASE noise has been effectively suppressed. Consequently, not only the wavelength down-conversion shown in Figs. 6(b)–6(d), but also the wavelength up-conversion shown in Fig. 4(a) and Fig. 6(a) are clearly observed in our proposed scheme.

4.2 Single-to-dual channel wavelength conversion

We then verify the single-to-dual channel wavelength conversion described in Fig. 2. The typical optical spectra of single-to-dual channel wavelength conversion are shown in Figs. 7(a)–7(d), which are just in accordance with Figs. 2(a)–2(d). Similar to Fig. 6, the signal and pump1 wavelengths are fixed at 1549.7 and 1536.6 nm, respectively. As shown in Figs. 7(a) and 7(b), when two pumps are close to each other, both pump1 and pump2 interact with the signal through the SFG process, generating two sum-frequency waves (SF1 and SF2). At the same time, pump2 and SF1, as well as pump1 and SF2, participate in the subsequent DFG process to yield two channel idler waves (idler2 and idler1). Figs. 7(c) and 7(d) also show the single-to-dual channel wavelength conversion as the wavelength of pump2 is tuned near the signal wavelength. However, different from Figs. 7(a) and 7(b) in which, SFG only occurs between the signal and the pump, here the SFG interaction takes place not only between the signal and one pump, but also between the two pumps. That is, both the two kinds of cSFG/DFG are employed in Figs. 7(c) and 7(d).

We further investigate the single-to-dual channel wavelength conversion in detail when fixing the signal and pump2 wavelengths while tuning the wavelength of pump1 as shown in Fig. 8. The wavelengths of the signal and pump2 waves are kept at 1549.7 and 1552.9 nm. The pump1 and pump2 powers at the output of the PPLN waveguide are measured at about 5.52 and 8.10 dBm, respectively. It is interesting to find that, idler1 is first smaller than idler2 as shown in Fig. 8(a),

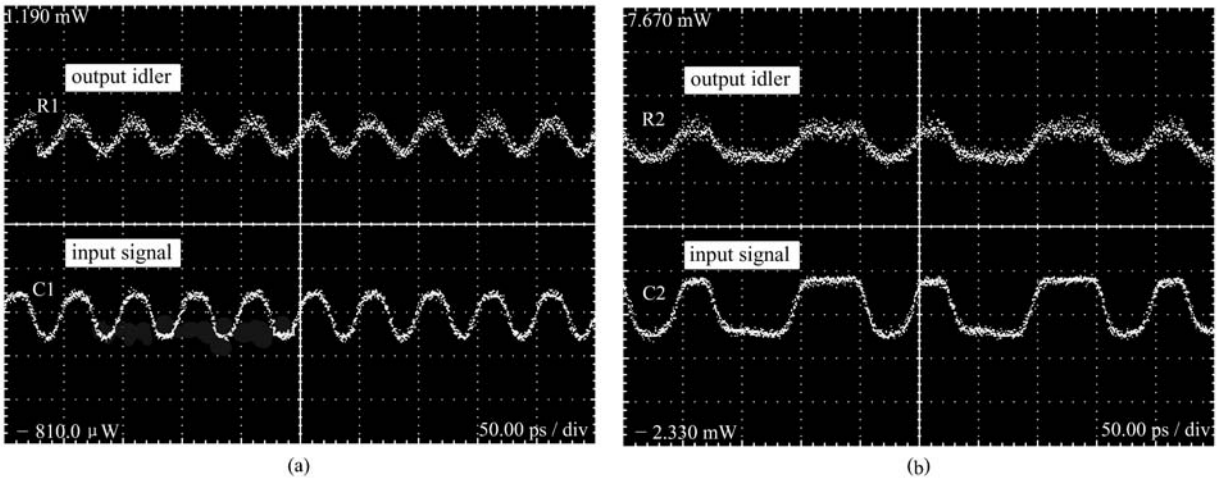

Fig. 5 Temporal waveforms for input signal (C1, C2) and output idler (R1, R2) waves at 40 Gbit/s with different bit stream. (a) "1 0 1 0 1 0 1 0"; (b) "1 0 0 0 1 1 0 0"

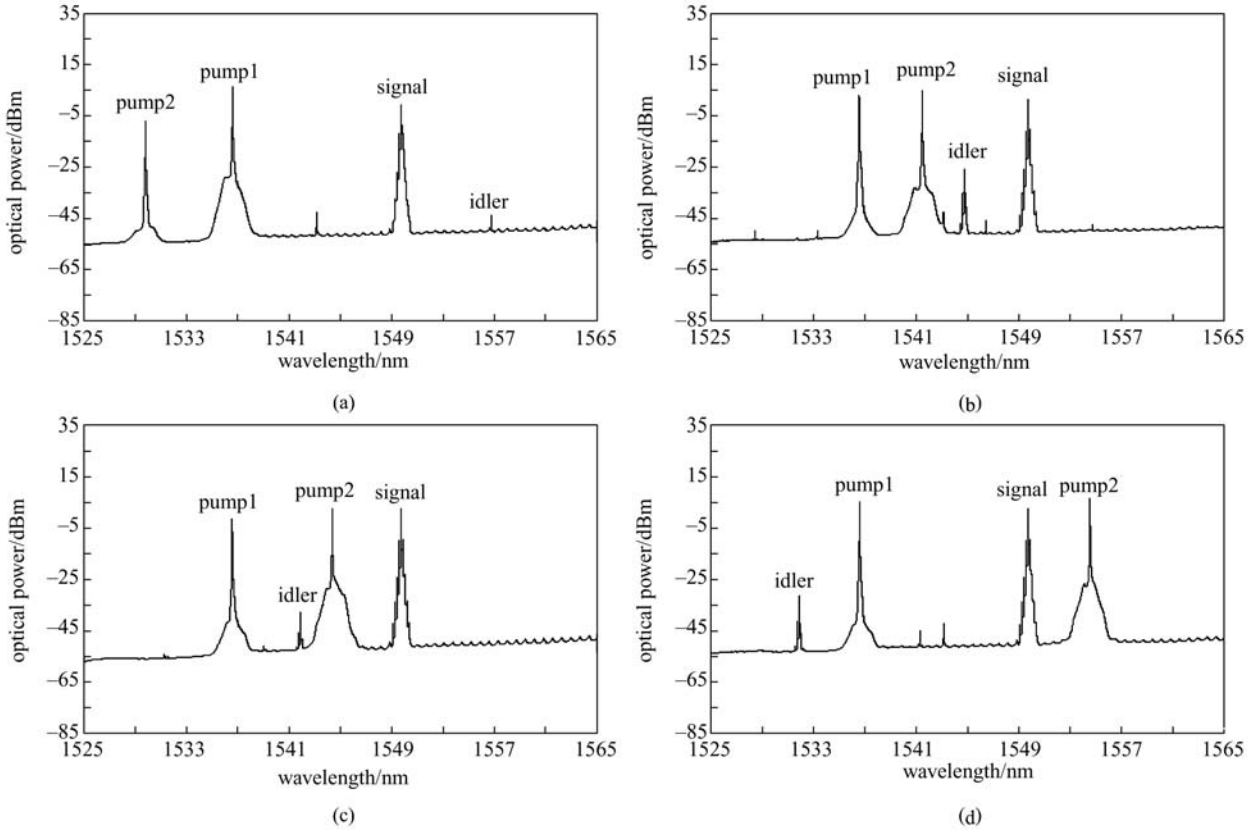

Fig. 6 Tunable performance of cSFG/DFG-based wavelength conversion. (a) $\lambda_{P2} = 1529.8$ nm, $\lambda_i = 1556.8$ nm; (b) $\lambda_{P2} = 1541.5$ nm, $\lambda_i = 1544.8$ nm; (c) $\lambda_{P2} = 1544.4$ nm, $\lambda_i = 1541.9$ nm; (d) $\lambda_{P2} = 1554.5$ nm, $\lambda_i = 1531.9$ nm

then almost the same as idler2 as shown in Figs. 8(b) and 8(c), and finally becomes larger than idler2 as shown in Fig. 8(d). To explain such phenomenon, we plot in Fig. 9(a) the measured conversion efficiencies of two channel idler waves as a function of the pump1 wavelength, from which we can obtain the following useful information.

Points A – D represent Figs. 8(a) – 8(d), respectively:

1) When the wavelength of pump1 is small ($\lambda_{P1} < 1534.4$ nm), the SFG process between pump1 and the signal (SFG1), as well as between pump1 and pump2 (SFG2), are both phase-mismatched, i.e.,

$$\Delta k_{SFG1} = 2\pi\left(\frac{n_{P1}}{\lambda_{P1}} + \frac{n_S}{\lambda_S} - \frac{n_{SF}}{\lambda_{SF}} + \frac{1}{\Lambda}\right) \neq 0,$$

$$\Delta k_{SFG2} = 2\pi\left(\frac{n_{P1}}{\lambda_{P1}} + \frac{n_{P2}}{\lambda_{P2}} - \frac{n_{SF}}{\lambda_{SF}} + \frac{1}{\Lambda}\right) \neq 0,$$

where n_k (k = P1, P2, S, SF) represent the refractive indexes for different wavelengths, and Λ is the microdomain period of the PPLN waveguide. Furthermore, $\Delta k_{SFG1} > \Delta k_{SFG2}$, thus, idler1 is smaller than idler2.

2) When $\lambda_{P1} \approx 1534.4$ nm, SFG1 is still phase-mismatched, while SFG2 is quasi-phase matched, i.e., $\Delta k_{SFG1} \neq 0$, $\Delta k_{SFG2} \approx 0$. Idler2 obtains its maximum and idler1 is smaller than idler2.

3) When 1534.4 nm $< \lambda_{P1} <$ 1535.3 nm, SFG2 becomes phase-mismatched again. It fulfills $\Delta k_{SFG1} > \Delta k_{SFG2} \neq 0$ and idler1 is smaller than idler2.

4) When 1535.3 nm $< \lambda_{P1} <$ 1536.6 nm, although both SFG1 and SFG2 are still phase-mismatched, $\Delta k_{SFG1} \approx \Delta k_{SFG2} \neq 0$. Therefore, idler1 is almost the same as idler2.

5) When 1536.6 nm $< \lambda_{P1} <$ 1537.6 nm, $0 \neq \Delta k_{SFG1} < \Delta k_{SFG2}$, and idler1 becomes larger than idler2.

6) When $\lambda_{P1} \approx 1537.6$ nm, SFG2 is phase-mismatched, while SFG1 is quasi-phase matched, i.e., $\Delta k_{SFG2} \neq 0$, $\Delta k_{SFG1} \approx 0$. Idler1 obtains its maximum and is larger than idler2.

7) When $\lambda_{P1} > 1537.6$ nm, SFG1 is phase mismatched-again. It obeys $0 \neq \Delta k_{SFG1} < \Delta k_{SFG2}$ and idler1 is larger than idler2.

Figure 9(b) depicts the conversion efficiency difference between the two channel idler waves as a function of the pump1 wavelength, from which, as described above, it can be concluded as below. When $\lambda_{P1} <$ 1535.3 nm, idler1 is smaller than idler2, which is shown in Fig. 8(a) (A in Fig. 9). When 1535.3 nm $< \lambda_{P1} <$ 1536.6 nm, idler1 is nearly equal to idler2, which is shown in Fig. 8(b) (B in Fig. 9) and Fig. 8(c) (C in Fig. 9). When $\lambda_{P1} >$ 1536.6 nm, idler1 is larger than idler2, which is shown in Fig. 8(d) (D in Fig. 9).

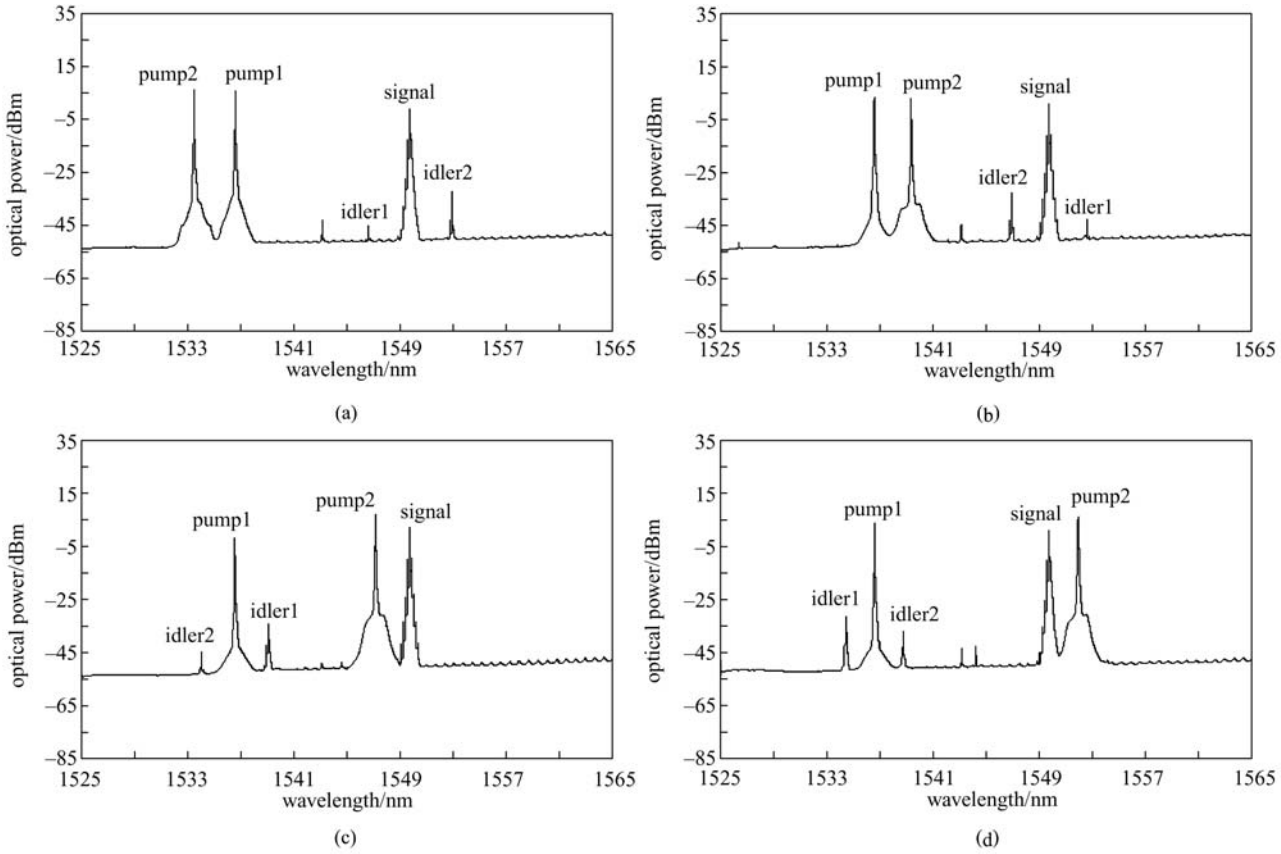

Fig. 7 Optical spectra of cSFG/DFG-based single-to-dual channel wavelength conversion. (a) $\lambda_{P2} = 1533.5$ nm, $\lambda_{i1} = 1546.6$ nm, $\lambda_{i2} = 1552.9$ nm; (b) $\lambda_{P2} = 1539.3$ nm, $\lambda_{i1} = 1552.6$ nm, $\lambda_{i2} = 1546.9$ nm; (c) $\lambda_{P2} = 1547.2$ nm, $\lambda_{i1} = 1539.1$ nm, $\lambda_{i2} = 1534.0$ nm; (d) $\lambda_{P2} = 1552.0$ nm, $\lambda_{i1} = 1534.4$ nm, $\lambda_{i2} = 1538.8$ nm

Actually, as shown in Figs. 9(a) and 9(b), the measured conversion efficiencies of idler1 and idler2 are not always identical with each other even though $1535.3\ \text{nm} < \lambda_{P1} < 1536.6\ \text{nm}$. Such fluctuation can be ascribed to the influences of random polarization states, the power and wavelength jitter of the optical sources, and the instabilities of the environment. In addition, for the fixed signal wavelength at 1549.7 nm, the pump1 wavelength in Figs. 4(a), 6, and 7 is 1536.6 nm, but becomes 1537.6 nm or thereabout under the QPM condition for the SFG process as shown in Figs. 8(d) and 9. This can be attributed to the variation of the QPM wavelength of the PPLN waveguide under the influence of the environment, as Figs. 4(a), 6, 7 and Figs. 8, 9 are measured during different time periods. However, this does not affect studying the dependence of two channel idler conversion efficiencies on the wavelength of pump1.

Wavelength relationships between two channel converted idler waves (λ_{i1}, λ_{i2}) and three incident waves (λ_S, λ_{P1}, λ_{P2}) are also studied theoretically and experimentally.

For Figs. 2(c) and 2(d), Figs. 7(c) and 7(d) and Fig. 8, since both two channel idler waves and three incident waves are within the 1.5-μm band, Eqs. (6) and (7) can be written as

$$\text{Channel 1:} \quad \lambda_{i1} \approx \lambda_S + \lambda_{P1} - \lambda_{P2}, \tag{8}$$

$$\text{Channel 2:} \quad \lambda_{i2} \approx \lambda_{P1} + \lambda_{P2} - \lambda_S. \tag{9}$$

From Eqs. (8) and (9), we can obtain

$$(\lambda_{i1} + \lambda_{i2})/2 = \lambda_{P1}, \tag{10}$$

$$|\lambda_{i1} - \lambda_{i2}| = 2|\lambda_S - \lambda_{P2}|. \tag{11}$$

According to Eqs. (8)–(11), we can find following conclusions.

1) From Eqs. (8) and (9), it is found that both two channel idler wavelengths change linearly with the wavelength of pump1, i.e., $\lambda_{i1} \propto \lambda_{P1}$, $\lambda_{i2} \propto \lambda_{P1}$. This can be clearly seen in Fig. 10(a).

2) From Eq. (10), it is found that the wavelengths of two channel idler waves are symmetric relative to the pump1 wavelength. Figure 10(b) shows the average wavelength of two channel idler waves, which is also linear with the wavelength of pump1 with a slope of 1. Figure 10(c) shows the difference between the average

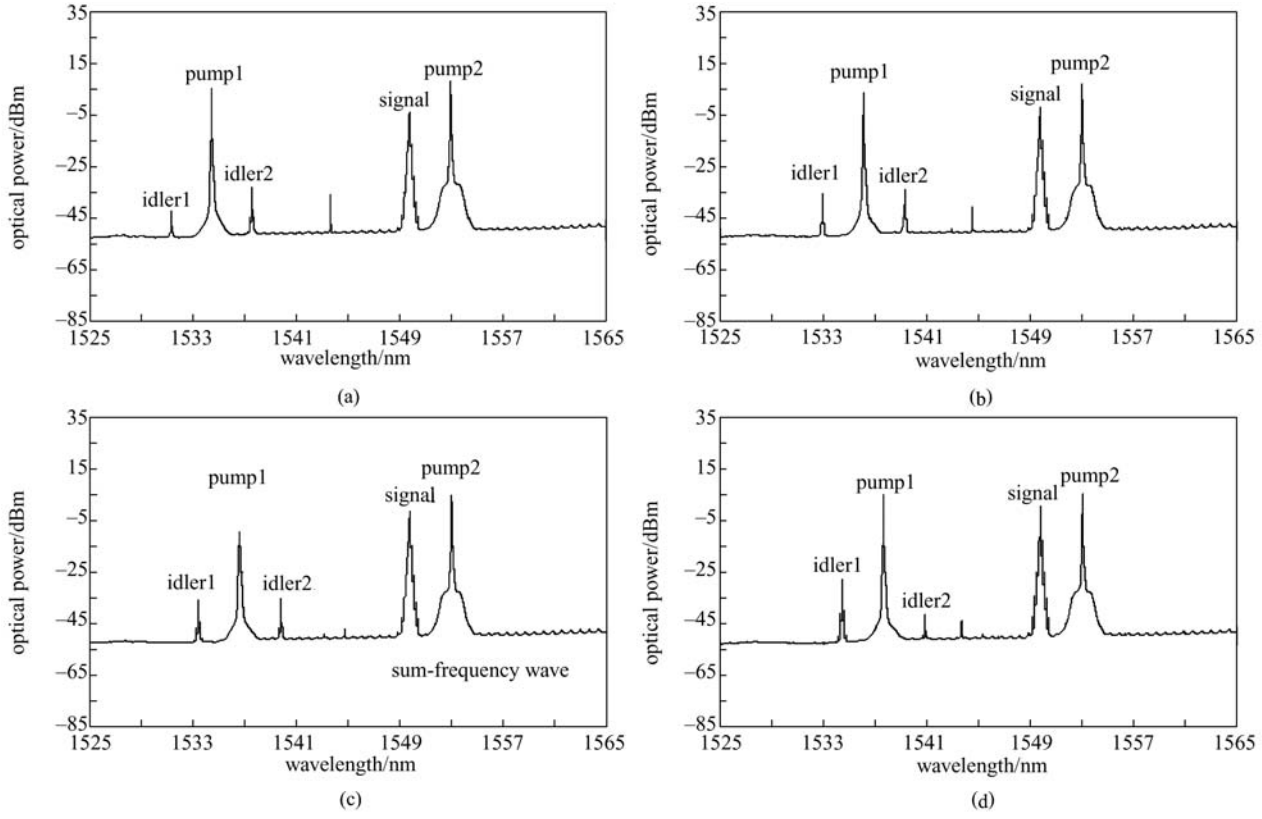

Fig. 8 Optical spectra of cSFG/DFG-based single-to-dual channel wavelength conversion when tuning the wavelength of pump1. (a) $\lambda_{P1} = 1534.4$ nm, $\lambda_{i1} = 1531.3$ nm, $\lambda_{i2} = 1537.6$ nm; (b) $\lambda_{P1} = 1536.1$ nm, $\lambda_{i1} = 1532.9$ nm, $\lambda_{i2} = 1539.3$ nm; (c) $\lambda_{P1} = 1536.6$ nm, $\lambda_{i1} = 1533.4$ nm, $\lambda_{i2} = 1539.8$ nm; (d) $\lambda_{P1} = 1537.6$ nm, $\lambda_{i1} = 1534.4$ nm, $\lambda_{i2} = 1540.8$ nm

wavelength of two channel idler waves and pump1 wavelength $[(\lambda_{i1} + \lambda_{i2})/2 - \lambda_{P1}]/\lambda_{P1}$ when tuning the wavelength of pump1. Obviously, from Figs. 10(b) and 10(c), we can confirm the above conclusions as deduced from Eq. (10).

3) From Eq. (11), it is found that the channel spacing between two channel idler waves is two times that of the spacing between the signal and the pump2 wavelengths. This is also successfully verified in Fig. 10(d), in which $|\lambda_{i1} - \lambda_{i2}| \approx 6.4\ \text{nm} = 2 \times 3.2\ \text{nm} = 2|\lambda_S - \lambda_{P2}|$.

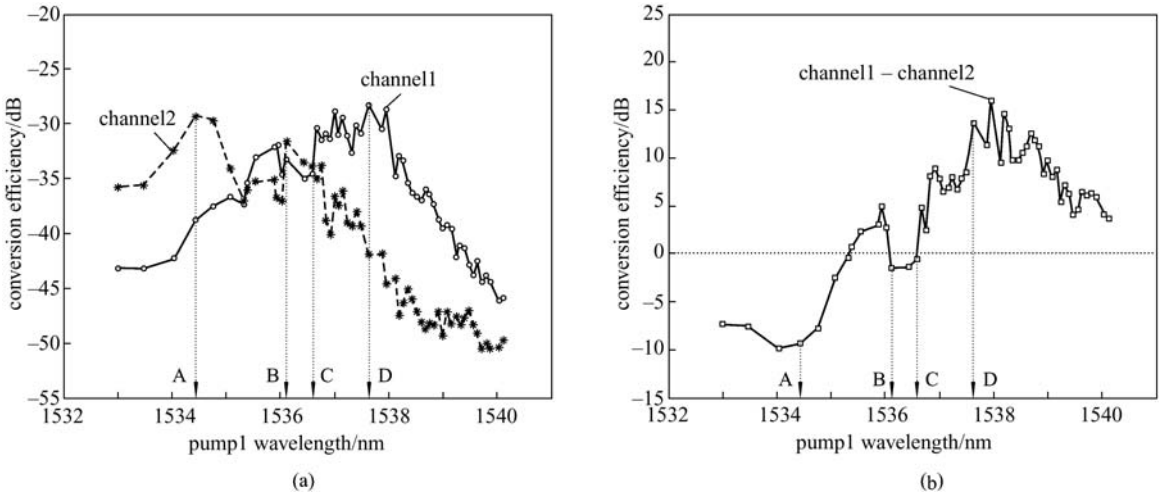

Fig. 9 Conversion efficiencies and conversion efficiency difference of the two channel idler waves versus pump1 wavelength. The signal and pump2 wavelengths are fixed at 1549.7 and 1552.9 nm, respectively. (a) Measured conversion efficiencies of two channel idler waves; (b) conversion efficiency difference between two channel idler waves

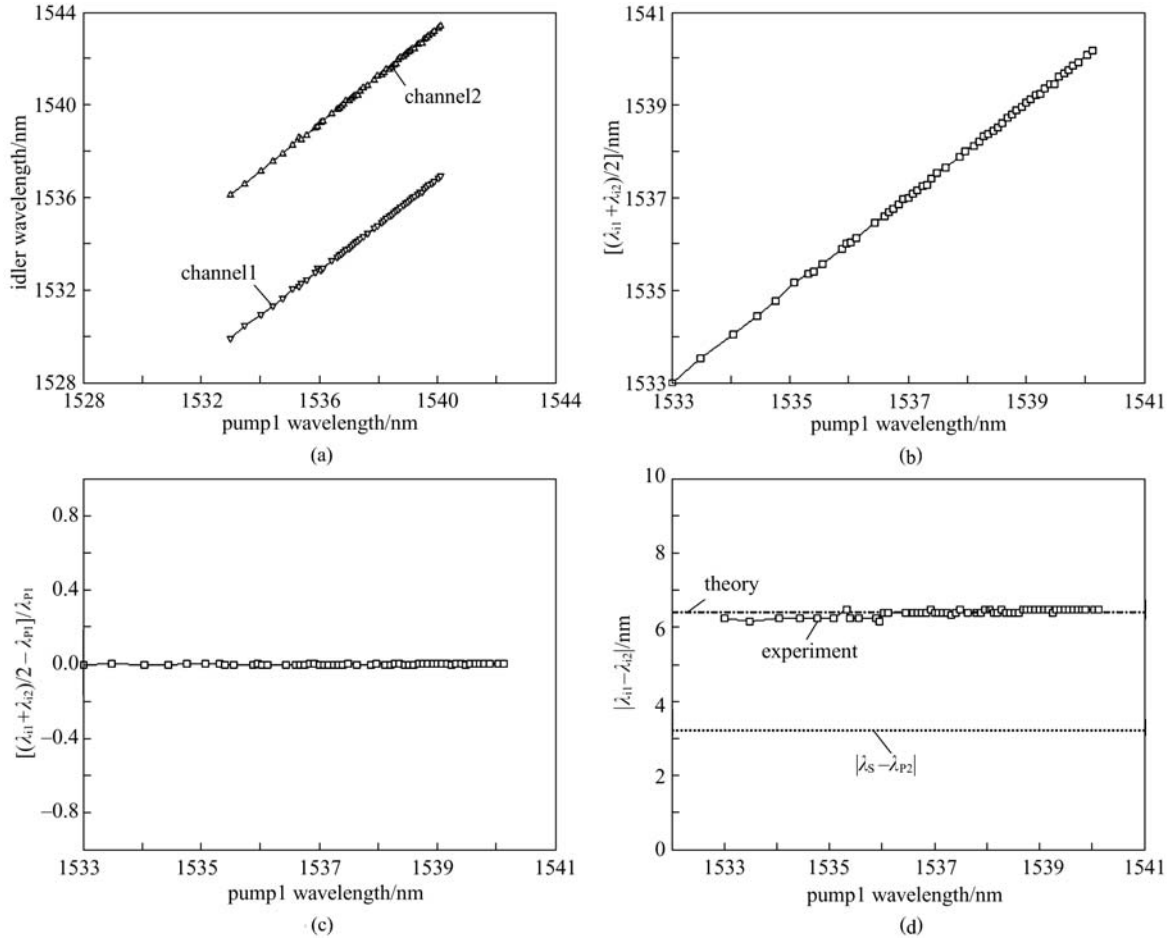

Fig. 10 Wavelength relationships between two channel converted idler waves and three incident waves. (a) Two channel idler wavelengths versus pump1 wavelength; (b) average wavelength of idler1 and idler2 versus pump1 wavelength; (c) difference between average wavelength of two idlers and pump1 wavelength versus pump1 wavelength; (d) channel spacing of idler1 and idler2 versus pump1 wavelength

Based on the above discussions, for a fixed input signal wavelength, it is expected that two channel idler wavelengths can be tuned by changing the wavelength of pump1, while the channel spacing between two channel idler wavelengths can be controlled by adjusting the pump2 wavelength.

Similarly, for Figs. 2(a) and 2(b) and Figs. 7(a) and 7(b), Eqs. (4) and (5) can be written as:

$$\text{Channel 1:}\quad \lambda_{i1} \approx \lambda_S + \lambda_{P2} - \lambda_{P1}, \tag{12}$$

$$\text{Channel 2:}\quad \lambda_{i2} \approx \lambda_S + \lambda_{P1} - \lambda_{P2}. \tag{13}$$

From Eqs. (12) and (13), we can obtain:

$$(\lambda_{i1} + \lambda_{i2})/2 = \lambda_S, \tag{14}$$

$$|\lambda_{i1} - \lambda_{i2}| = 2|\lambda_{P1} - \lambda_{P2}|. \tag{15}$$

Therefore, two channel idler wavelengths are symmetrically relative to the signal wavelength, and the channel spacing between two channel idler wavelengths is two times that of the spacing between two pump wavelengths.

Conventional cSFG/DFG scheme employs two HP-EDFAs to amplify two CW pumps, respectively. In our proposed scheme, according to the existing lab conditions, only one HP-EDFA is employed. In the configuration, two tunable filters are utilized and the ASE noise caused by HP-EDFA is successfully suppressed. As a consequence, single-to-single channel tunable wavelength down- and up-conversions are simultaneously observed, single-to-dual channel wavelength conversion is also experimentally verified, and two kinds of cSFG/DFG schemes are both demonstrated.

5 Conclusions

By exploiting cSFG/DFG in a PPLN waveguide, we have proposed and demonstrated 40 Gbit/s single-to-single and single-to-dual channel wavelength conversion with

two pump configuration. Firstly, only one HP-EDFA and two tunable filters are employed. The ASE noise is effectively suppressed. As a result, tunable wavelength down- and up-conversions are simultaneously observed. The converted idler wavelength is tuned from 1556.8 to 1531.9 nm as the wavelength of pump2 is changed from 1529.8 to 1554.5 nm, covering a 24.9-nm conversion span. Secondly, single-to-dual channel wavelength conversion is experimentally verified when two pumps or one pump and the signal are close to each other. We place focus on the latter, in which two kinds of cSFG/DFG schemes are both included and simultaneously observed. It is found that idler1 is smaller than idler2 when $\lambda_{P1} < 1535.3$ nm, then becomes almost the same as idler2 when $1535.3\ \text{nm} < \lambda_{P1} < 1536.6$ nm, and is larger than idler2 when $\lambda_{P1} > 1536.6$ nm. Moreover, the wavelength relationships between two channel idler waves and three incident waves are studied both theoretically and experimentally, showing that two channel idler wavelengths are symmetric relative to the pump1 wavelength, and the channel spacing is two times that of the spacing between the signal and pump2 wavelengths. The proposed scheme could be applied in practical wavelength conversion applications to enhance the flexibility of future optical networks.

Acknowledgements This work was supported by the National Natural Science Foundation of China (Grant No. 60577006) and the Program for New Century Excellent Talents in University, Ministry of Education of China (Grant No. NCET-04-0694). The authors would like to thank Dr. J. R. Kurz and Prof. M. M. Fejer of Stanford University for fabricating the PPLN waveguide for the experiments.

References

1. Yoo S J B. Wavelength conversion technologies for WDM network applications. Journal of Lightwave Technology, 1996, 14(6): 955–966
2. Xu C Q, Okayama H, Kawahara M. 1.5 μm band efficient broadband wavelength conversion by difference frequency generation in a periodically domain-inverted $LiNbO_3$ channel waveguide. Applied Physics Letters, 1993, 63(26): 3559–3561
3. Chou M H, Hauden J, Arbore M A, et al. 1.5-μm-band wavelength conversion based on difference-frequency generation in $LiNbO_3$ waveguides with integrated coupling structures. Optics Letters, 1998, 23(13): 1004–1006
4. Zhou B, Xu C Q, Chen B. Comparison of difference-frequency generation and cascaded $\chi^{(2)}$ based wavelength conversions in $LiNbO_3$ quasi-phase-matched waveguides. Journal of the Optical Society of America B–Optical Physics, 2003, 20(5): 846–852
5. Chou M H, Brener I, Fejer M M, et al. 1.5-μm-band wavelength conversion based on cascaded second-order nonlinearity in $LiNbO_3$ waveguides. IEEE Photonics Technology Letters, 1999, 11(6): 653–655
6. Schreiber G, Suche H, Lee Y L, et al. Efficient cascaded difference frequency conversion in periodically poled Ti: $LiNbO_3$ waveguides using pulsed and CW pumping. Applied Physics B–Lasers and Optics, 2001, 73(5–6): 501–504
7. Xu C Q, Bracken J, Chen B. Intracavity wavelength conversions employing a MgO-doped $LiNbO_3$ quasi-phase-matched waveguide and an erbium-doped fiber amplifier. Journal of the Optical Society of America B–Optical Physics, 2003, 20(10): 2142–2149
8. Sun Junqiang, Liu Wei, Tian Jian, et al. Multichannel wavelength conversion exploiting cascaded second-order nonlinearity in $LiNbO_3$ waveguides. IEEE Photonics Technology Letters, 2003, 15(12): 1743–1745
9. Sun Junqiang, Liu Wei. Multiwavelength generation by utilizing second-order nonlinearity of $LiNbO_3$ waveguides in fiber lasers. Optics Communications, 2003, 224(1–3): 125–130
10. Sun Junqiang, Ma Zetao, Liu Deming, et al. Wavelength conversion between picosecond pulses using cascaded second-order nonlinearity in $LiNbO_3$ waveguides. Optical and Quantum Electronics, 2005, 37(5): 443–456
11. Sun Junqiang, Yuan Xiuhua, Liu Deming. Tunable wavelength conversion between picosecond pulses using cascaded second-order nonlinearity in $LiNbO_3$ waveguides. Applied Physics B–Lasers and Optics, 2005, 80(6): 681–685
12. Wang Jian, Sun Junqiang, Li Jing, et al. Single-to-dual channel wavelength conversion of picosecond pulses using PPLN-based double-ring fibre laser. Electronics Letters, 2006, 42(4): 236–238
13. Wang Jian, Sun Junqiang, Luo Chuanhong, et al. Single-to-multiple channel wavelength conversions and tuning of picosecond pulses in quasi-phase-matched waveguides. Chinese Physics Letters, 2006, 23(7): 1806–1809
14. Asobe M, Yokohama I, Itoh H, et al. All-optical switching by use of cascading of phase-matched sum-frequency-generation and difference-frequency-generation processes in periodically poled $LiNbO_3$. Optics Letters, 1997, 22(5): 274–276
15. Yokohama I, Asobe M, Yokoo A, et al. All-optical switching by use of cascading of phase-matched sum-frequency generation and difference-frequency generation processes. Journal of the Optical Society of America B–Optical Physics, 1997, 14(12): 3368–3377
16. Min Y H, Lee J H, Lee Y L, et al. Tunable all-optical wavelength conversion of 5 ps pulses by cascaded sum- and difference frequency generation (cSFG/DFG) in a Ti:PPLN waveguide. In: Proceedings of Optical Fiber Communications Conference (OFC'03), Atlanta. 2003, 2: 767–768
17. Yamawaku J, Takada A, Yamazaki E, et al. Selective wavelength conversion using PPLN waveguide with two pump configuration. In: Proceedings of Conference on Lasers and Electro-Optics, Jun., 1-6, 2003: 1135–1136
18. Lee Y L, Jung C, Noh Y-C, et al. Channel-selective wavelength conversion and tuning in periodically poled Ti: $LiNbO_3$ waveguides. Optics Express, 2004, 12(12): 2649–2655
19. Lee Y L, Yu B-A, Jung C, et al. All-optical wavelength conversion and tuning by the cascaded sum- and difference frequency generation (cSFG/DFG) in a temperature gradient controlled Ti:PPLN channel waveguide. Optics Express, 2005, 13(8): 2988–2993
20. Yu S, Gu W. A tunable wavelength conversion and wavelength add/drop scheme based on cascaded second-order nonlinearity with double-pass configuration. IEEE Journal of Quantum Electronics, 2005, 41(7): 1007–1012
21. Xu C Q, Chen B. Cascaded wavelength conversions based on sum-frequency generation and difference-frequency generation. Optics Letters, 2004, 29(3): 292–294
22. Chen B, Xu C Q. Analysis of novel cascaded $\chi^{(2)}$ (SFG + DFG) wavelength conversions in quasi-phase-matched waveguides. IEEE Journal of Quantum Electronics, 2004, 40(3): 256–261
23. Yu S, Gu W. Wavelength conversions in quasi-phase matched $LiNbO_3$ waveguide based on double-pass cascaded $\chi^{(2)}$

SFG + DFG interactions. IEEE Journal of Quantum Electronics, 2004, 40(11): 1548–1554
24. Wang Jian, Sun Junqiang, Luo Chuanhong, et al. Experimental demonstration of wavelength conversion between ps-pulses based on cascaded sum- and difference frequency generation (SFG + DFG) in $LiNbO_3$ waveguides. Optics Express, 2005, 13(19): 7405–7414
25. Wang Jian, Sun Junqiang. All-optical single-to-dual channel wavelength conversion based on sum-frequency generation and difference-frequency generation. Microwave and Optical Technology Letters, 2006, 48(10): 2057–2060
26. Wang Jian, Sun Junqiang. Observation of 40-Gbit/s tunable wavelength down- and up-conversions based on cascaded second-order nonlinearity in $LiNbO_3$ waveguides. Optical Engineering, 2007, 46(2): 025005
27. Wang Jian, Sun Junqiang, Kurz J R, et al. Tunable wavelength conversion of ps-pulses exploiting cascaded sum- and difference frequency generation in a PPLN-fiber ring laser. IEEE Photonics Technology Letters, 2006, 18(20): 2093–2095
28. Wang Jian, Sun Junqiang, Luo Chuanhong, et al. Flexible all-optical wavelength conversions of 1.57-ps pulses exploiting cascaded sum- and difference frequency generation (cSFG/DFG) in a PPLN waveguide. Applied Physics B–Lasers and Optics, 2006, 83(4): 543–548
29. Wang Jian, Sun Junqiang, Zhang Xinliang, et al. Experimental observation of tunable wavelength down- and up-conversions of ultra-short pulses in a periodically poled $LiNbO_3$ waveguide. Optics Communications, 2007, 269(1): 179–187